Supporting Information for

Dual-functional device based on CB/PVDF@BFP for solar-driven water purification and water-induced electricity generation

*Jiangchao Huang,[‡a] Veronica Pereira,[‡b] Chenyue Wang, [‡a] Haitao Li,[*a] Hiang Kwee Lee,[*b,c] and Jie Han,[*a]*

[a]*School of Chemistry and Chemical Engineering, Yangzhou University, Yangzhou, 225002, PR China.*

[b]*Division of Chemistry and Biological Chemistry, School of Chemistry, Chemical Engineering and Biotechnology, Nanyang Technological University, 21 Nanyang Link, Singapore 637371.*

[c] *Institute of Materials Research and Engineering, The Agency for Science, Technology and Research (A*STAR), 2 Fusionopolis Way, #08-03, Innovis, 138634, Singapore.*

‡ These authors contributed equally to this work.

Corresponding Author

E-mail address: htli@yzu.edu.cn (Haitao Li); hiangkwee@ntu.edu.sg (Hiang Kwee Lee); hanjie@yzu.edu.cn (Jie Han)

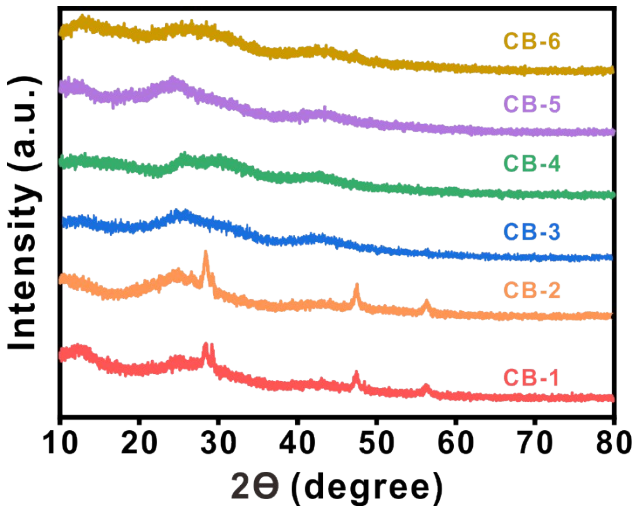

Fig. S1. XRD patterns of CB with various particle sizes. CB-1: 1000 mesh, CB-2: 2000 mesh, CB-3: 3000 mesh, CB-4: 4000 mesh, CB-5: 4500 mesh, and CB-6: 5000.

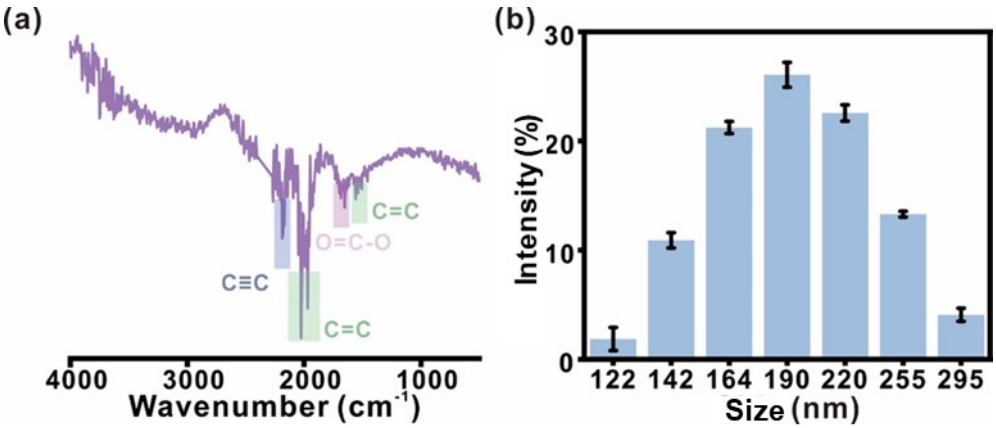

Fig. S2. (**a**) FTIR spectrum and (**b**) particle size distribution of CB powder (4500 mesh).

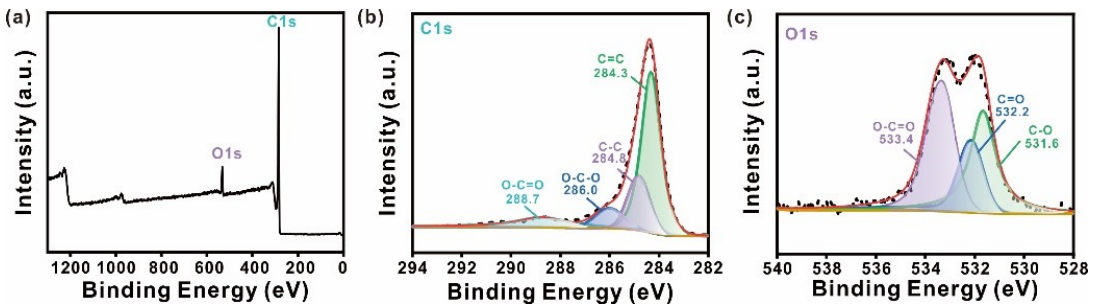

Fig. S3. (**a**) Survey XPS spectrum and (**b, c**) high-resolution C 1s and O 1s XPS spectra of CB powders (4500 mesh), respectively.

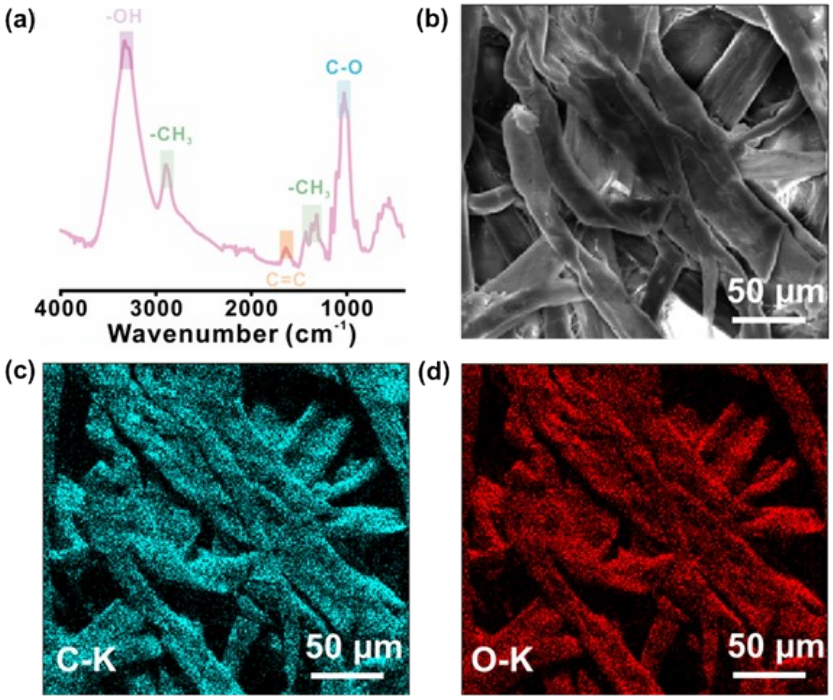

Fig. S4. (**a**) FTIR spectra of BFP. (**b, c, d**) EDS elemental mapping of C and O elements of the BFP.

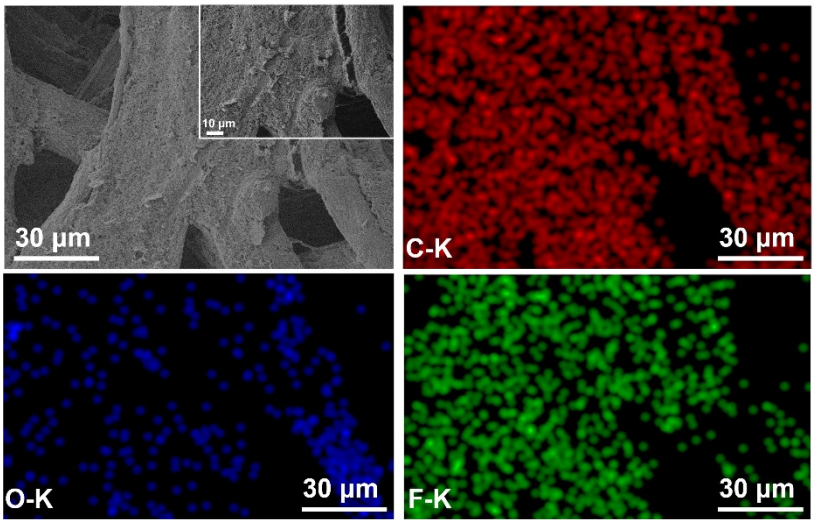

Fig. S5. EDS elemental mapping of C, O and F elements of the CB/PVDF@BFP.

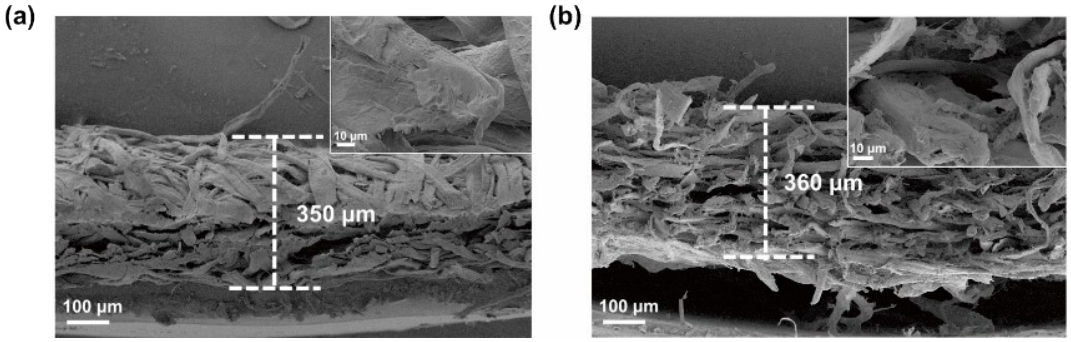

Fig. S6. Cross-sectional SEM images of **(a)** BFP and **(b)** CB/PVDF@BFP. Insets, Corresponding high magnification SEM image.

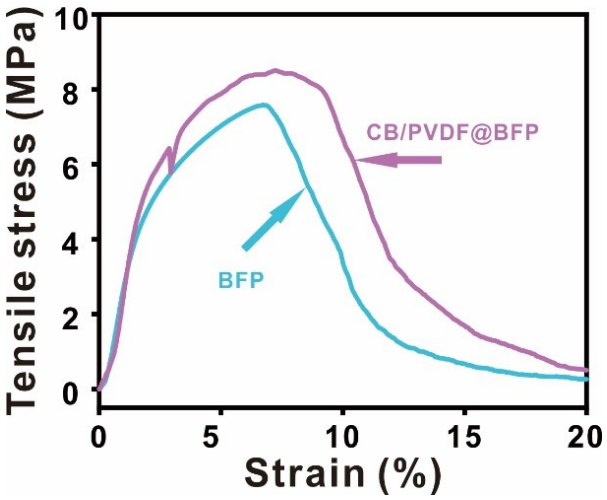

Fig. S7. Tensile strain-stress curve of the BFP with dimensions of 70× 30× 0.35 mm^3 and CB/PVDF@BFP with dimensions of 70× 30× 0.36 mm^3.

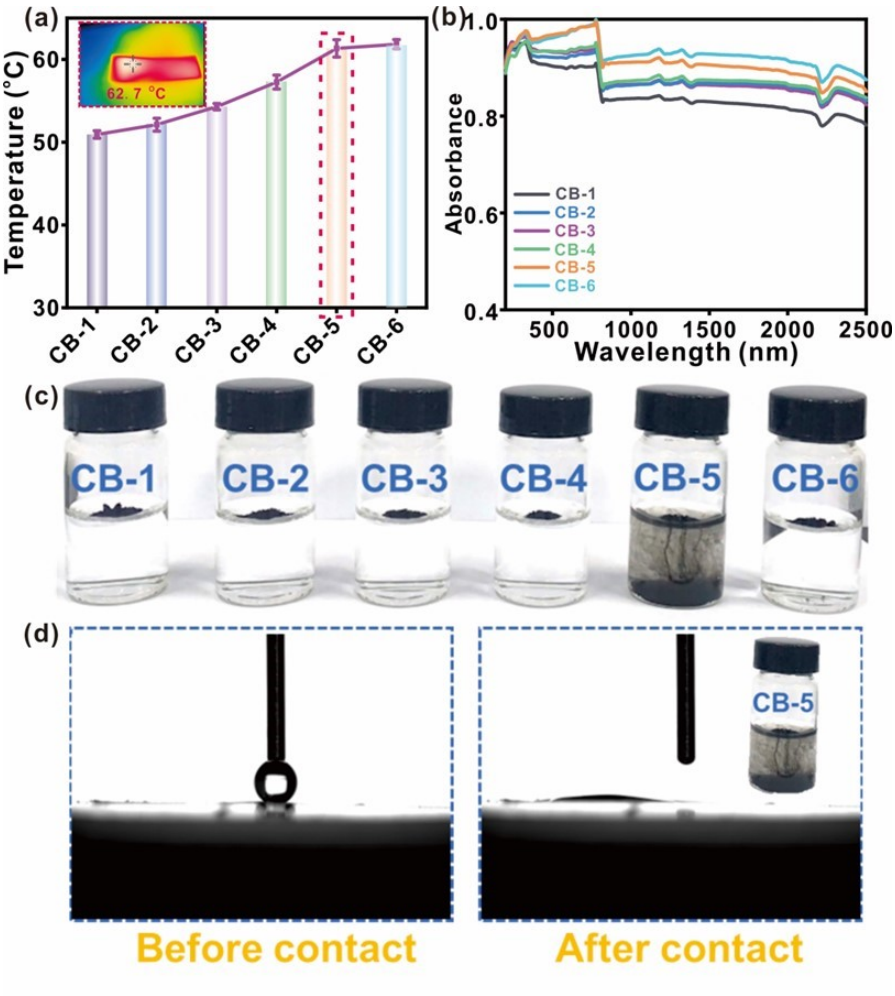

Fig. S8. CB/BFP with various CB sizes (1000-5000 mesh). (**a**) Photothermal surface temperature under 1 sun irradiation, (**b**) UV-vis-NIR absorption spectra, and (**c**) water solubility test. (**d**) Water contact angle images when a water droplet is placed on CB-5 (4500 mesh).

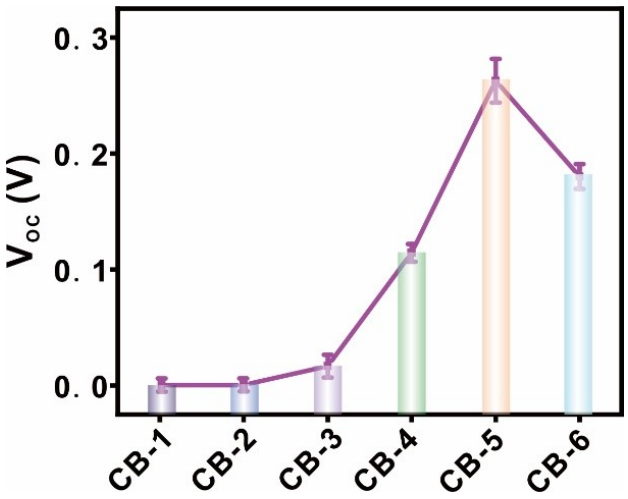

Fig. S9. V_{OC} of CB/BFP with various CB sizes (1000-5000 mesh).

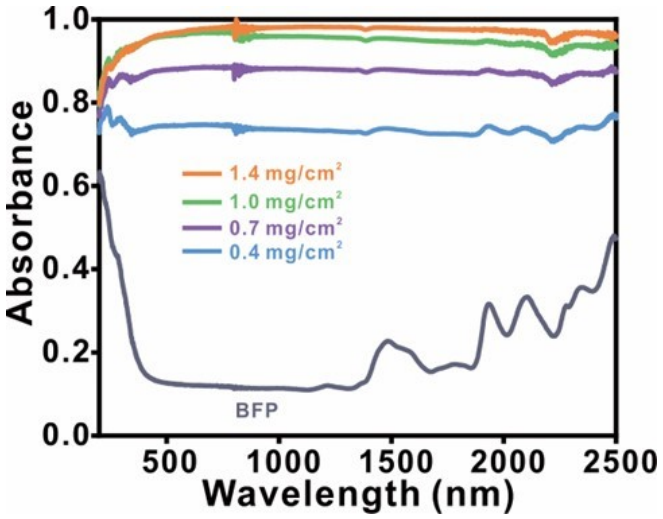

Fig. S10. UV-Vis-NIR spectra of BFP and CB/PVDF@BFP with different areal loading density (0.4-1.4 mg/cm^2).

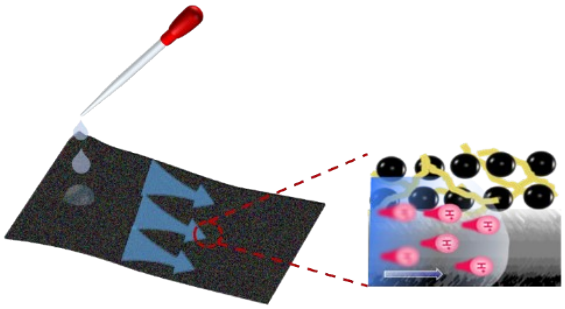

Fig. S11. Illustration of power generation mechanism of the CB/PVDF@BFP.

When a water drop is dispensed onto the device, the water will flow from the wet side of the CB/PVDF@BFP to the dry side via capillary flow within the highly hydrophilic BFP. During such water transfer process, positively charged protons and solvated cations on the liquid side and electrons on the solid side of the carbon/water interface are transported by the capillary flow of water. Such directional movement of electrical charges thus create a pseudostreaming current that can be harvested to generate electrical power. It is also noteworthy that protons are continuously migrating from the wet side to the dry side owing to the formation of a water content gradient across the device, thereby enabling consistent electrical outputs (V_{OC} and I_{SC}) until the water is fully evaporated.

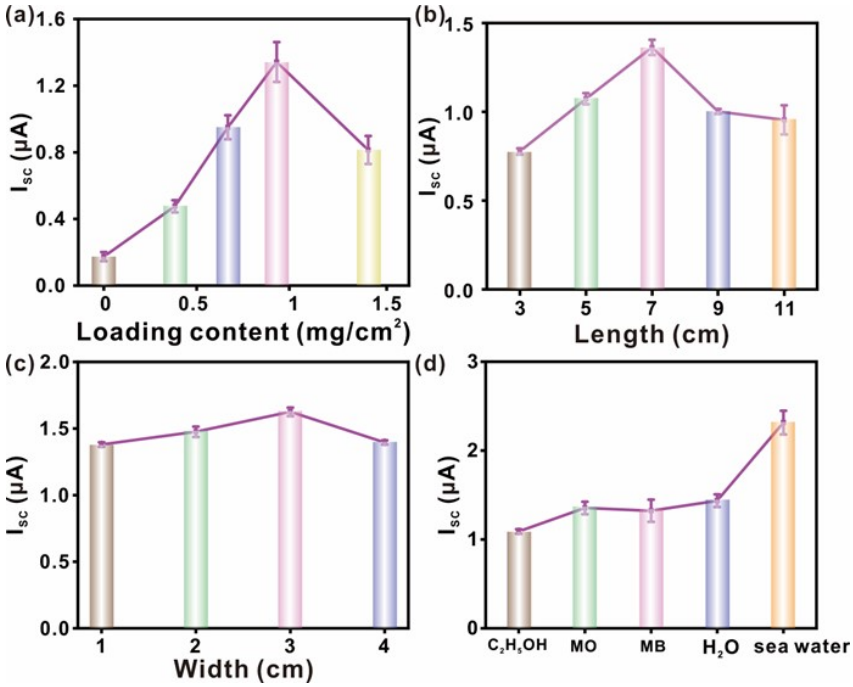

Fig. S12. I_{SC} of CB/PVDF@BFP with different (**a**) areal loading density, (**b**) device length (3-11 cm), (**c**) device width (1-4 cm), and (**d**) solutions as test liquid under 1 sun irradiation.

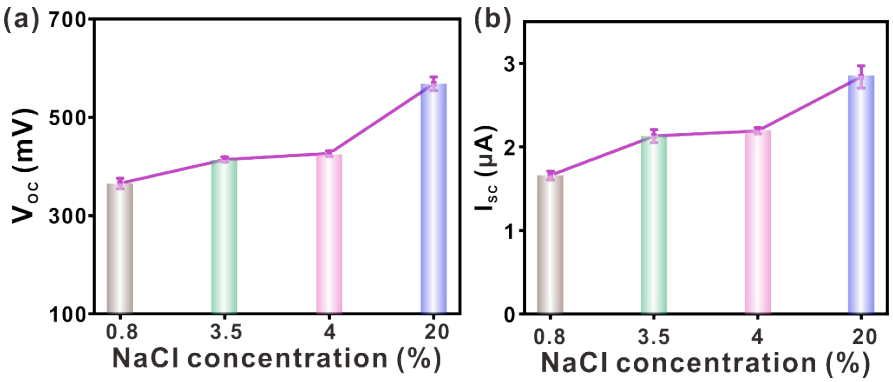

Fig. S13. V_{OC} and I_{SC} of CB/PVDF@BFP when tested with four different artificial seawater samples under 1 sun irradiation.

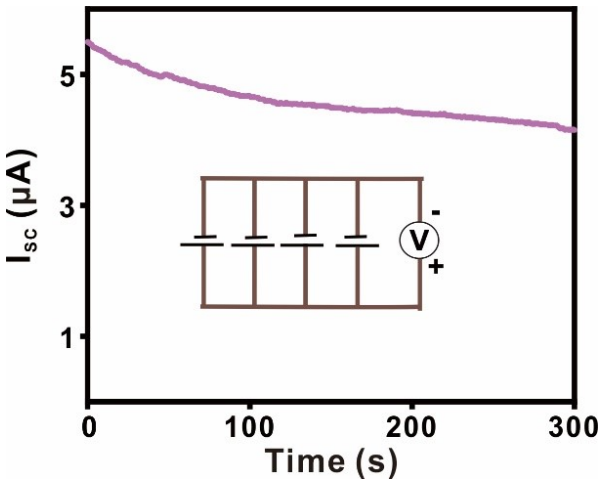

Fig. S14. I_{SC} recorded when four CB/PVDF@BFP platforms are connected in parallel under 1 sun irradiation.

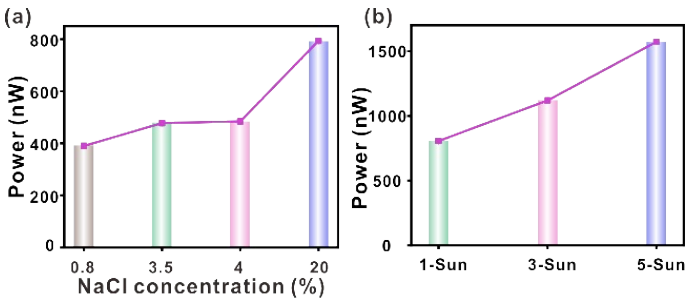

Fig. S15. The maximal output power of the CB/PVDF@BFP platform quantified (load resistance, 2 MΩ) under **(a)** four different artificial seawater samples, and **(b)** different solar irradiation (1-5 sun). All experiments are performed under 50 RH% and 25 ℃.

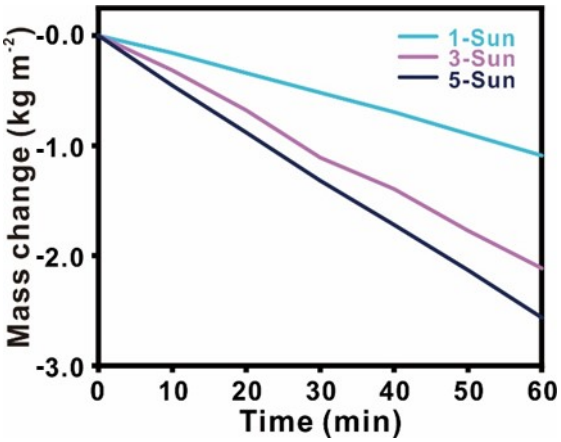

Fig. S16. Temporal mass change of seawater solution when treated with CB/PVDF@BFP under solar irradiation (1-5 sun).

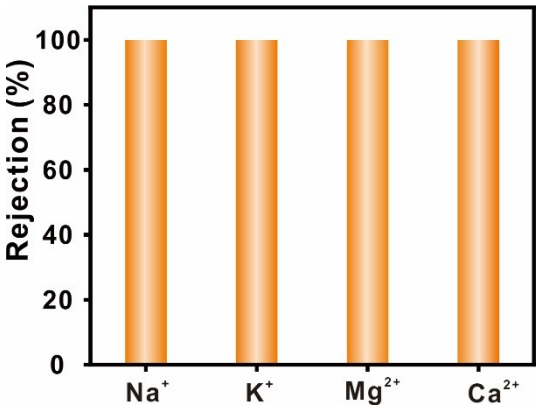

Fig. S17. Rejection rates (i.e., desalination efficiency) of salt ions via solar-driven water evaporation using CB/PVDF@BFP platform.

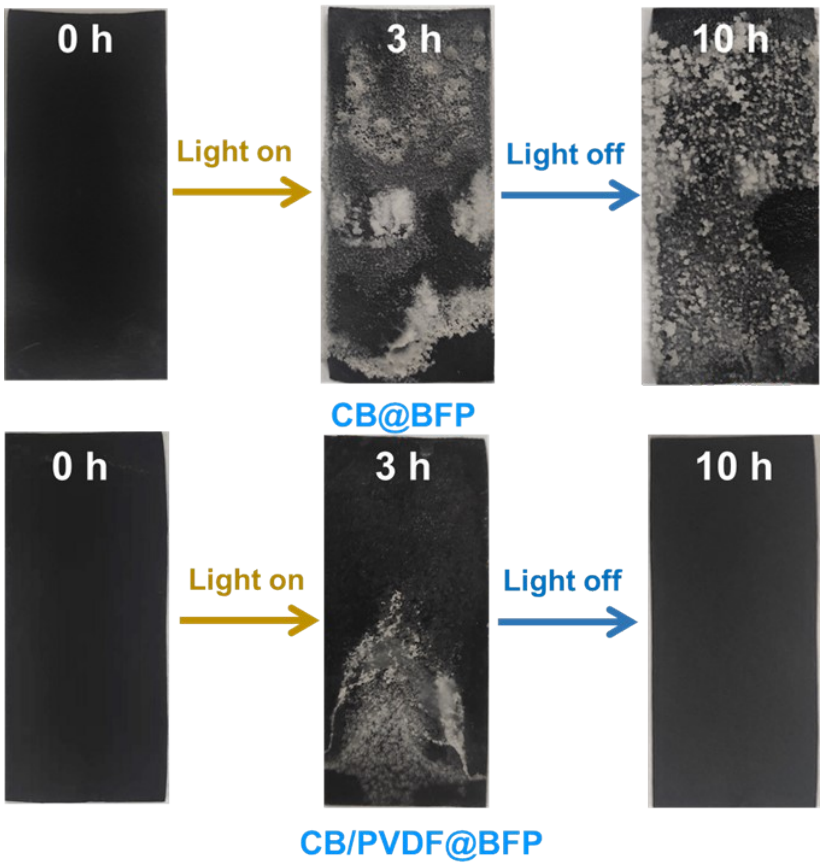

Fig. S18. Photographs showing salt crystals blocking different types of material surfaces after 10 h of solar irradiation (1 sun) in a 20% NaCl solution.

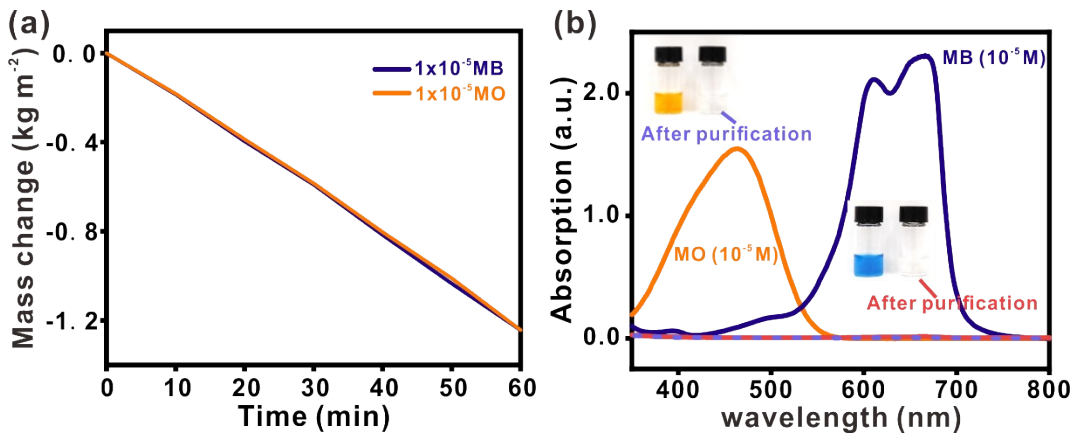

Fig. S19. (a) Time-dependent mass change of aqueous MO and MB solutions by using CB/PVDF@BFP under 1 sun irradiation. **(b)** Absorption spectra of aqueous MO and MB solutions (10^{-5} M) before and after treatment.

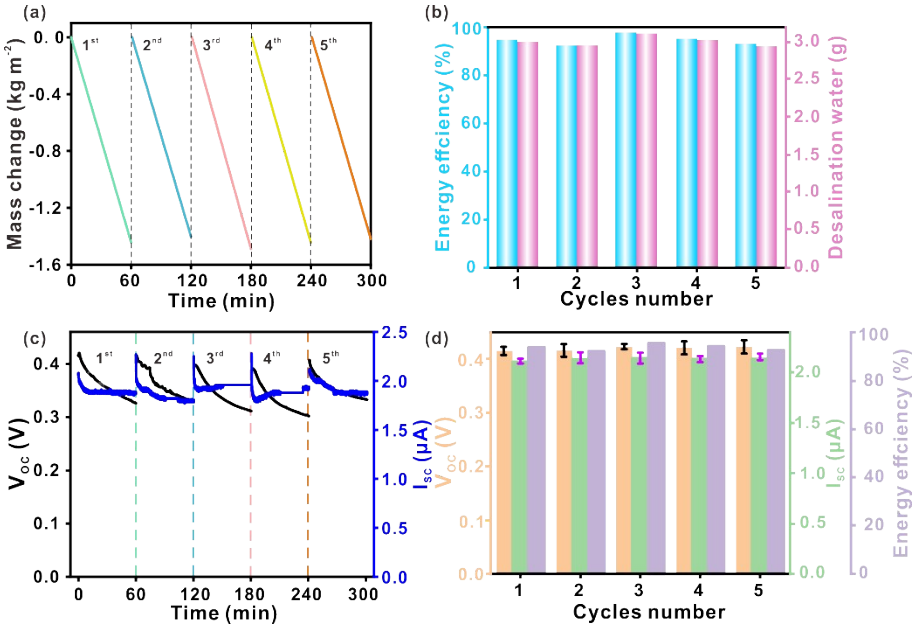

Fig. S20. (a) Temporal mass change of seawater over five cycle tests when treated with CB/PVDF@BFP film under one sun irradiation. (b) Corresponding energy efficiency and the collected mass of desalinated water over five cycles. (c) Trends of V_{OC} and I_{SC} output over five repeated cycles. (d) V_{OC}, I_{SC} and energy efficiency of our device over five test cycles. All experiments are conducted under 50 RH% and 25 ℃.

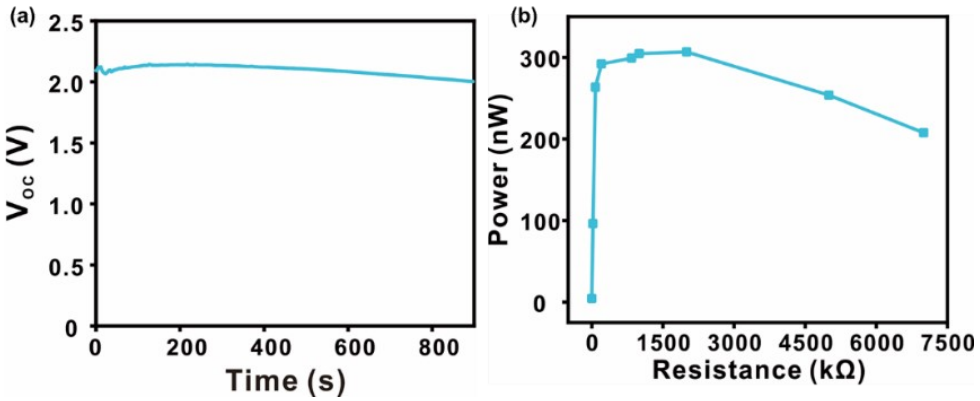

Fig. S21. (a) V_{OC} of the dual-functional device in seawater and **(b)** output power of the CB/PVDF@BFP platform under 1 sun irradiation and 25 °C.

Table S1. Comparison of evaporation rate of our work with the reported literatures.

Material	Category	Water Evaporation Rate (kg m^{-2} h^{-1})	Ref.
CB/PMMA-PAN	Carbonaceous	1.30	[1]
F-wood/CNTs	Carbonaceous	0.95	[2]
Flame-treated	Carbonaceous	1.05	[3]
Carbon particles	Carbonaceous	0.96	[4]
RGO-SA-CNT	Carbonaceous	1.39	[5]
rGO-MWCNT	Carbonaceous	1.22	[6]
2D g-CNS_{TC}	Carbonaceous	1.30	[7]
CB/PVDF@BFP	Carbonaceous	1.436	This work

References

[1] W. Xu, X. Hu, S. Zhuang, Y. Wang, X. Li, L. Zhou, S. Zhu and J. Zhu, Adv. Energy Mater., 2018, **8**, 1702884.

[2] M. Xie, J. Qian, Y. Li, H. Yang, J. Qu, X. Hu and Q. Mao, Appl. Opt., 2021, **60**, 4930-4937.

[3] G. Xue, K. Liu, Q. Chen, P. Yang, J. Li, T. Ding, J. Duan, B. Qi and J. Zhou, ACS Appl. Mater. Interfaces, 2017, **9**, 15052-15057.

[4] S. Liu, C. Huang, X. Luo and Z. Rao, Appl. Therm. Eng., 2018, **142**, 566-572.

[5] X. Hu, W. Xu, L. Zhou, Y. Tan, Y. Wang, S. Zhu and J. Zhu, Adv. Mater., 2017, **29**, 1604031.

[6] Y. Wang, C. Wang, X. Song, S.K. Megarajan and H. Jiang, J. Mater. Chem.A, 2018, **6**, 963-971.

[7] M. Aizudin, R. Goei, A.J. Ong, Y.Z. Tan, S.K. Lua, R.P. Pottammel, H. Geng, X.-L. Wu, A.L.Y. Tok and E.H. Ang, J. Mater. Chem.A, 2022, **10**, 19612-19617.